Accepted Manuscript

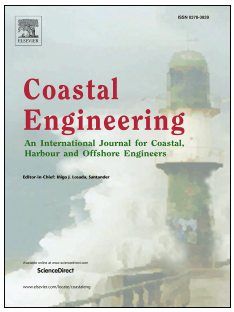

Combined wave-current induced excess pore-pressure in a sandy seabed: Flume observations and comparisons with theoretical models

Wen-Gang Qi, Chang-Fei Li, Dong-Sheng Jeng, Fu-Ping Gao, Zuodong Liang

PII: S0378-3839(18)30235-7

DOI: https://doi.org/10.1016/j.coastaleng.2019.02.006

Reference: CENG 3469

To appear in: *Coastal Engineering*

Received Date: 13 May 2018

Revised Date: 22 December 2018

Accepted Date: 11 February 2019

Please cite this article as: Qi, W.-G., Li, C.-F., Jeng, D.-S., Gao, F.-P., Liang, Z., Combined wave-current induced excess pore-pressure in a sandy seabed: Flume observations and comparisons with theoretical models, *Coastal Engineering* (2019), doi: https://doi.org/10.1016/j.coastaleng.2019.02.006.

Combined wave-current induced excess pore-pressure in a sandy seabed: Flume observations and comparisons with theoretical models

Wen-Gang Qi [a,b], Chang-Fei Li [a,b], Dong-Sheng Jeng[c], Fu-Ping Gao [a,b,*], Zuodong Liang[c]

[a] *Key Laboratory for Mechanics in Fluid Solid Coupling Systems, Institute of Mechanics, Chinese Academy of Sciences, Beijing 100190, China*
[b] *School of Engineering Science, University of Chinese Academy of Sciences, Beijing 100049, China*
[c] *School of Engineering and Built Environment, Griffith University, Gold Coast Campus, QLD4222, Australia*

ABSTRACT

Waves are coexisting with currents in coastal zones; nevertheless, previous experimental studies for excess pore-pressure responses in a porous seabed were predominantly limited to the wave-only condition. In this study, the combined wave-current induced excess pore-pressures in a sandy seabed were experimentally simulated with a specially-designed flume, which can concurrently generate periodic waves and a following/opposing co-directional current. The effect of a current on the wave profile is firstly examined. The wave steepness is decreased by a following current, but enhanced by an opposing current. Flume observations indicate that, under combined wave-current loading, the wave-induced pore-pressure is increased for the following-current case, but reduced for the opposing-current case. Such wave-current combination effect becomes more significant for shorter wave periods. The variation trend of the excess pore-pressure distribution in the present flume observations is consistent with that of the existing analytical solutions. Nevertheless, due to the existence of wave and/or current boundary layer and non-lineartiy of wave-current interactions as indicated by the flume observations, certain deviations exist between the flume results for excess pore-pressure and the analytical solutions, which can not be ignored especially for the opposing-current case. The effects of the boundary layer on the combined wave-current induced pore-pressures in the seabed are further highlighted by supplementary numerical simulations. A favorable prediction by the analytical solution would be expected for following-current cases and smaller pore-pressure amplitudes would be obtained for opposing-current cases.

Keywords: Excess pore-pressure; flume experiment; sandy seabed; combined waves and current; boundary layer; wave-current interactions

[*] Corresponding author. *E-mail address*: fpgao@imech.ac.cn (Fu-Ping Gao)

This manuscript is the 2nd revised version to ***Coastal Engineering*** *(Short Communication)* for review

1. Introduction

The evaluation of the wave-induced soil response in marine sediments is particularly important for the design of foundations of offshore installations such as wind turbine foundations (Cuéllar, 2012; Lin et al., 2017), platforms (Bea et al., 1983; Zhang et al., 2017), pipelines (de Groot and Meijers, 1992; Zhou et al., 2015) and breakwaters (Oumeraci, 1994; Zhang and Ge, 1996; de Groot et al., 2006; Liao et al., 2018a, 2018b). Therefore, it is necessary to have a better understanding of the wave-induced pore-pressure in marine sediments.

In the past a few decades, numerous analytical solutions have been obtained and several experimental works have been done for wave-induced oscillatory pore-pressure responses. Based on Biot's poro-elastic theory, a few porous models for wave-seabed interactions were ever established under various assumptions (see Sumer, 2014; Jeng, 2018). Among these, the analytical solution by Yamamoto et al. (1978) took into account of compressible pore-water in a compressible isotropic porous seabed with infinite thickness. Madsen (1978) presented a general analytical solution for pore-pressures and effective stresses in a hydraulically anisotropy porous seabed with infinite thickness. With the same framework, Hsu and Jeng (1994) later derived the analytical solution to Biot's equations for the case of finite soil thickness, which can converge to the above solution by Yamamoto et al. (1978) and Madsen (1978) if the soil thickness approaches infinity. The validity of these analytical solutions have been confirmed by both one-dimensional tests using cylindrical-shaped apparatuses (Chowdhury et al., 2006; Liu et al., 2015) and flume experiments (Tsui and Helfrich, 1983; Chang et al., 2007; Zhang et al., 2016; Zhai et al., 2018). A detailed review of the previous investigations on the wave-seabed interaction can be found in Jeng (2003; 2013; 2018).

In natural ocean environments, waves are coexisting with currents. The pore-pressure responses of the seabed could be significantly different when a current is considered. To the author's knowledge, Ye and Jeng (2012) were the first ones to study the soil response for the scenario of combined waves and currents. Numerical simulations were conducted based on

Biot's poro-elastic dynamic theory (*u-p* approximation). Their results showed that the maximum relative difference of the pore-pressure between the cases with currents and without currents can reach up to 25%. Zhang et al. (2013) proposed an analytical approximation for the evaluation of the pore-pressure in the seabed under combined waves and currents by adopting an updated wave-induced pressure at the seabed surface. It indicated that the influence of a current on the pore-pressure responses is significant. The full dynamic soil behavior was considered by Liao et al. (2013) and an analytical solution of the pore-pressure responses was derived for an infinite seabed. The parametric study showed that the current with third-order wave loading and full dynamic soil behavior cannot be ignored in the estimation of the wave-induced seabed responses for nearly-saturated soil, long-wave periods, and shallow water. Wen et al. (2016) established a three-dimensional numerical model for pore-pressure response under combined short-crested waves and currents. The numerical results indicated that superimposing a following-current will result in larger pore-pressure in the seabed. Therefore, ignoring a following-current would underestimate the wave-induced seabed instability.

As aforementioned analytical and numerical studies indicated, while considering the combined wave-current induced pore-pressure responses in a seabed, the Biot's poroelastic theory (Biot, 1941, 1960) is accepted as the principle of compressible pore fluid flow in a compressive porous medium. The governing equations of seabed responses are the same for wave-only condition and combined wave-current condition. Consequently, the essential difference of the pore-pressures between wave-only condition and combined wave-current condition is induced by the different boundary conditions of pressure at the seabed surface. This highlights the significance of the effect of wave-current interaction on the pressure distributions at the seabed surface. However, despite a substantial amount of knowledge has accumulated about the effect of wave-current interactions on the velocity profiles and turbulence characteristics (e.g. Kemp and Simons, 1982, 1983; Zhang et al., 2014; Tambroni et al., 2015; Singh and Debnath, 2016), little attention has been paid to the effect of wave-current interaction on the pressure distributions at the seabed surface. Moreover, the existing

studies with respect to combined wave-current induced pore-pressure responses in the seabed were predominantly limited to deriving analytical solutions and conducting numerical simulations. A systematic experimental study on the excess pore-pressure responses under combined waves and current has not been available in the literature. Note that the "excess pore-pressure" herein denotes the wave-induced pore-pressure relative to the still hydrostatic pressure in the seabed (refer to Yamamoto et al., 1978; Zen and Yamazaki, 1990).

In the present study, a series of large flume tests were conducted to investigate the excess pore-pressure responses in a sandy seabed under combined waves and current. To examine the effect of wave-current combination on the excess pore-pressure responses, various magnitudes of the following-current and the opposing-current were superimposed on the waves. The variation of the excess pore-pressure responses with wave period were investigated for the conditions of wave-only and combined waves and current. Moreover, the applicability of the existing analytical solution was examined by comparing the excess pore-pressure distributions between the experimental results and the existing analytical solutions. Several numerical simulations were also carried out to elucidate the significant effects of boundary layer on the combined wave-current induced pore-pressures in the seabed.

2. Experimental study

2.1. Experimental set-up

The combined wave-current induced excess pore-pressure responses in a sandy seabed were experimentally simulated with a specially-designed flume, which can concurrently generate periodic waves and a following/opposing co-directional current. The major frame of the flume is 52.0 m in length, 1.0 m in width and 1.5 m in depth, in the middle of which a soil-box of 2.0 m (length)×0.5 m (depth)×1.0 m (width) was constructed for the sand-bed preparation, as illustrated in Fig. 1.

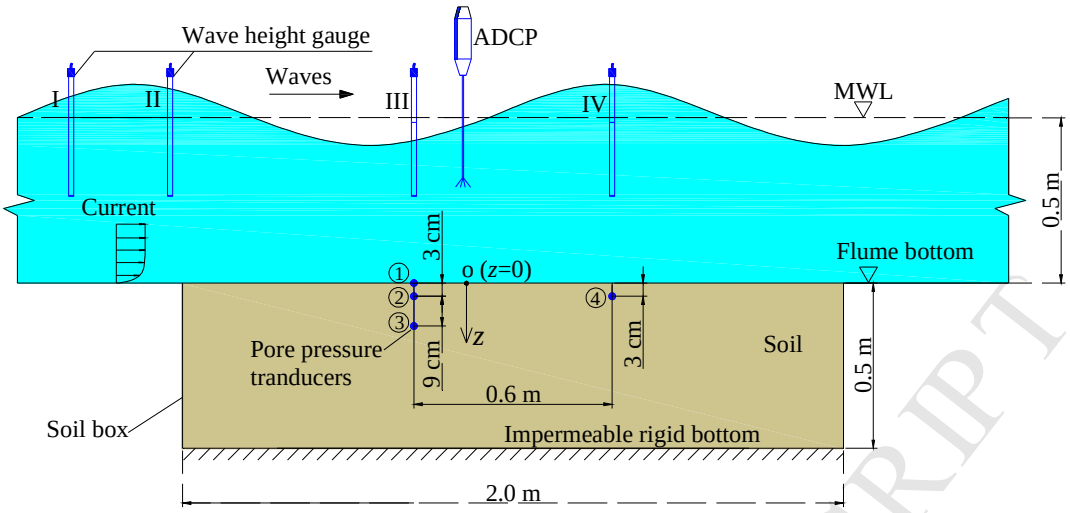

Fig. 1. Schematic diagram of the flume tests for combined wave-current induced excess pore-pressure in a sandy seabed.

A sandy seabed was prepared with a sand-raining device, whose main physical properties are listed in Table 1. Four miniature pore-pressure transducers (PPTs) with model number of GE Druck PDCR 81 were utilized to measure the wave-induced pore-pressure in the soil, as detailed in Fig. 1. Two wave height gauges (WHGs; model number: LYL-2) developed by Dalian University of Technology were located just above the PPTs. Far-field wave height was measured with the other two WHGs to guarantee the accuracy and reliability of the measured wave height and calculated wave length. The measurement accuracy of WHGs is 1 millimeter. The signals of WHGs and PPTs were multichannel synchronous sampled via the data acquisition card (NI USB-6211) with a sampling frequency of 100 Hz. An ADCP (model number: Vectrino-II; sampling volume: 0.085 cm^3; sampling frequency: 100 Hz) was mounted to measure the flow velocity at the level of 0.5h (i.e., 0.25 m) above the sandy seabed near the PPTs.

Table 1. Index properties of test sands.

Mean size of sand grains	Geometric standard deviation	Coefficient of permeability	Void ratio	Relative density	Buoyant unit weight of soil
d_{50} (mm)	σ_g	k_s (m/s)	e	D_r	γ' (kN/m^3)

0.38	1.28	1.88×10^{-4}	0.771	0.352	9.32

2.2. Test procedure and test conditions

In general, the testing procedure was adopted as follows:

(1) The flume including the soil box was firstly emptied and cleaned.

(2) The PPTs were deaired and then saturated to ensure their argil-covers being free of air. They were then installed at the specific locations with the support of a rack (see Fig. 1).

(3) The soil box was filled with clean water to a certain depth. The sand bed was carefully prepared by means of sand-raining technique. The surface of the sand bed was leveled off smoothly with a scraper.

(4) The flume was then filled slowly with water to a given depth (0.5 m in the present tests).

(5) For the tests of wave-only, the piston-type wave maker was activated and progressive waves propagated from inlet onto the sandy seabed. For the tests of combined waves and current, the current generator was firstly switched on and the flow velocity was gradually increased to approach the target value. Thereafter, the wave maker was activated.

(6) The multichannel synchronous sampling system was then started to measure the multi-physics parameters including wave height, pore-pressure and flow velocity.

Test conditions for investigating the wave-current induced excess pore-pressure in a sandy seabed are summarized in Table 2. The mean water depth (h) was kept constant at 0.5 m. The wave period (T), wave height (H_0) and current velocity (U_c) were kept unchanged during the test for the same run number. Note that, H_0 is the wave height under wave-only; and U_c is the average velocity of the current without waves at the level of 0.25 m above the sandy seabed. g is the gravitational acceleration. ξ_0 ($=H_0/L_0$) is the wave steepness under wave-only, where L_0 is the wave length under wave-only. The value of L_0 can be obtained from the dispersion relationship:

$$L_0 = \frac{gT^2}{2\pi}\tanh(k_0 h) \tag{1}$$

where $k_0=2\pi/L_0$ is the wave number under wave-only. $\xi(=H/L)$ is the wave steepness considering the effect of current, where H and L are the wave height and wave length considering the effect of current, respectively. The values of H and L for calculating ξ are obtained from a theoretical expression for the variation of wave height and wave length with current velocity based on the linear theory of wave-current interaction (see Zou, 2004)

$$\frac{H}{H_0}=2\left(\chi+\chi^{1/2}\right)^{-1/2}\left(1+\chi^{1/2}\right)^{-1/2} \tag{2a}$$

$$\frac{L}{L_0}=\frac{1}{4}\left(1+\chi^{1/2}\right)^{2} \tag{2b}$$

in which $\chi=1+4U_c/c_0$, $c_0=L_0/T$ is the wave velocity under wave-only.

According to the diagram of "the range of suitability of various wave theories" proposed by Lé Mehauté (1976), wave conditions of this study mainly fall in Stokes third-order wave theory zones (as shown in Fig. 2).

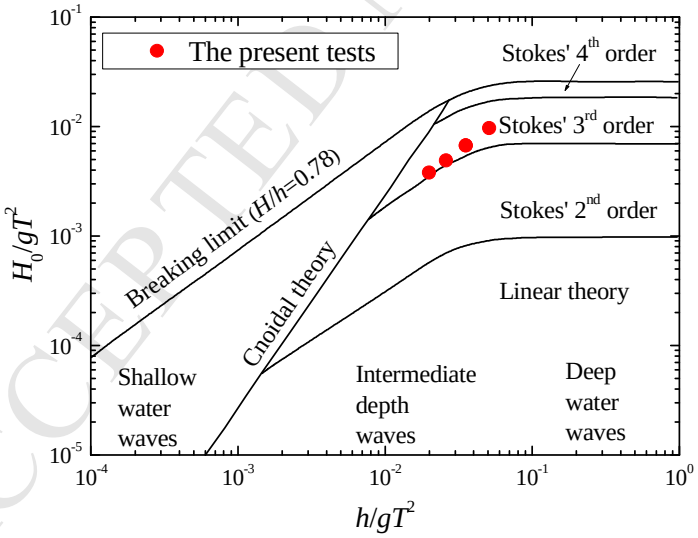

Fig. 2. Range of suitability of various wave theories (Lé Mehauté , 1976).

Supplementary tests were conducted to investigate the variation of wave height and wave length with the current velocity, and the profiles of flow velocity under various

hydrodynamic loading conditions. The test conditions for these supplementary tests are not elaborated in Table 2.

Table 2. Summary of test conditions for wave-current induced excess pore-pressure in a sandy seabed.

Run number	H_0 (cm)	T (s)	U_c (m/s)	H_0/gT^2	h/gT^2	ξ_0	ξ
1	9.5	1.2	0	0.0067	0.0354	0.046	0.046
2	9.5	1.2	0.1	0.0067	0.0354	0.046	0.037
3	9.5	1.2	0.2	0.0067	0.0354	0.046	0.031
4	9.5	1.2	0.3	0.0067	0.0354	0.046	0.027
5	9.5	1.2	-0.1	0.0067	0.0354	0.046	0.060
6	9.5	1.2	-0.2	0.0067	0.0354	0.046	0.084
7	9.5	1.2	-0.3	0.0067	0.0354	0.046	0.137
8	9.5	1.0	0	0.0097	0.0510	0.063	0.063
9	9.5	1.0	0.25	0.0097	0.0510	0.063	0.037
10	9.5	1.0	-0.25	0.0097	0.0510	0.063	0.167
11	9.5	1.2	0.25	0.0067	0.0354	0.046	0.029
12	9.5	1.2	-0.25	0.0067	0.0354	0.046	0.104
13	9.5	1.4	0	0.0049	0.0260	0.037	0.037
14	9.5	1.4	0.25	0.0049	0.0260	0.037	0.024
15	9.5	1.4	-0.25	0.0049	0.0260	0.037	0.077
16	9.5	1.6	0	0.0038	0.0199	0.031	0.031
17	9.5	1.6	0.25	0.0038	0.0199	0.031	0.020
18	9.5	1.6	-0.25	0.0038	0.0199	0.031	0.061

3. Results and discussions: Effects of imposing a current on waves

3.1. Variations of wave height and wave length

While waves and current coexist, the presence of a current will change the original wave height and wave length due to the interactions between waves and current. Fig. 3 shows the variation of the measured wave height and wave length with the velocity of the current (U_c, refer to Fig. 4). The theoretical results calculated with Eq. (2) are also given in Fig. 3.

Theoretical solutions of Eq. (2) assume a uniform current and a deep water condition (i.e. $\tanh(k_0h)\rightarrow 1.0$), while in the experiments there exists an obvious boundary layer in the current (see Fig. 4) and the value of $\tanh(k_0h)$ is approximately 0.92. In spite of these two deviations from the actual experimental condition, Fig. 3 shows that the theoretical results are generally consistent with the experimental results in the current velocity range of U_c>-0.1 m/s. The wave height decreases and the wave length elongates significantly with increasing

velocity of a following-current. In contrast, the wave height is augmented and the wave length gets shorter with increasing velocity of an opposing-current, i.e., an opposing-current induces wave steepening.

Note that the theoretical solutions tend to overestimate the opposing-current-induced increase of wave height and decrease of wave length, while the velocity of the opposing-current is relatively large (e.g. U_c=-0.22 & -0.28 m/s). This might be due to the nonlineartiy of wave-current interactions. Typical snapshots of the wave profiles under the conditions of U_c=-0.20 m/s and U_c=-0.30 m/s are shown in Fig. 5(b) and 5(c), respectively. As a reference, a snapshot of the wave profile under wave-only is also given in Fig. 5(a). It is observed that the wave profiles under U_c=-0.20 m/s and U_c=-0.30 m/s are no longer sinusoidal. The surface of the waves are wrinkled up and apt to break, which implies a significant non-lineartiy of wave-current interactions (see Moreira and Peregrine, 2012).

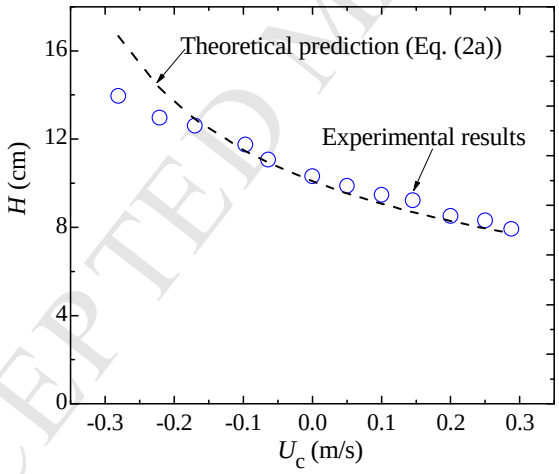

(a)

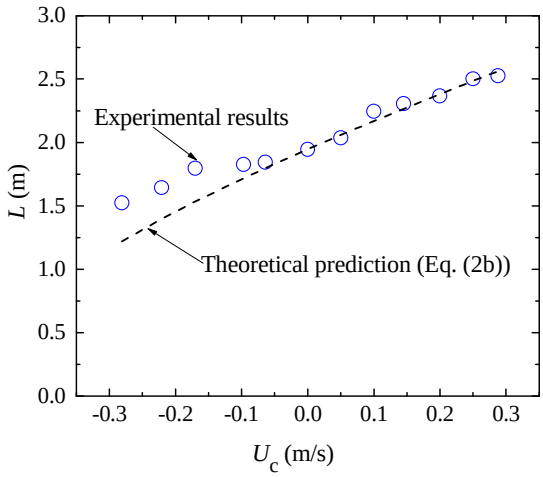

(b)

Fig. 3. Effect of a current on the (a) wave height H; and (b) wave length L. (Waves: h=0.5 m, T=1.2 s, H_0=10.2 cm).

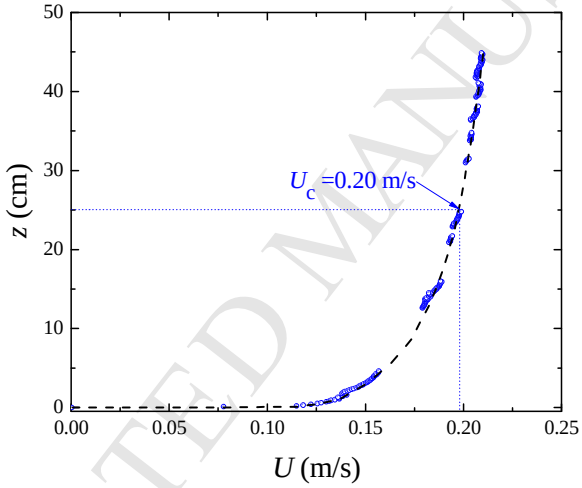

Fig. 4. Measured velocity profile of a unidirectional current.

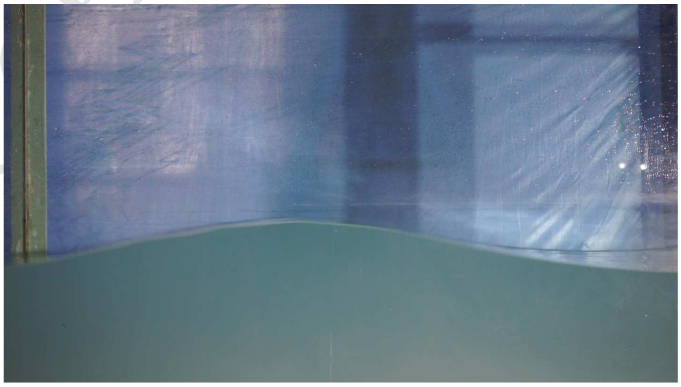

(a) Wave-only

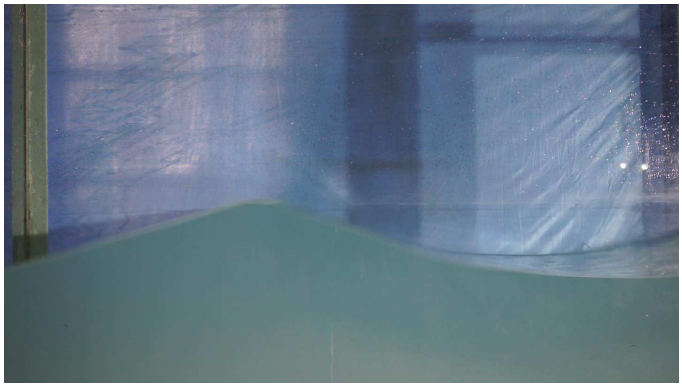

(b) Wave with an opposing current (U_c=-0.20 m/s)

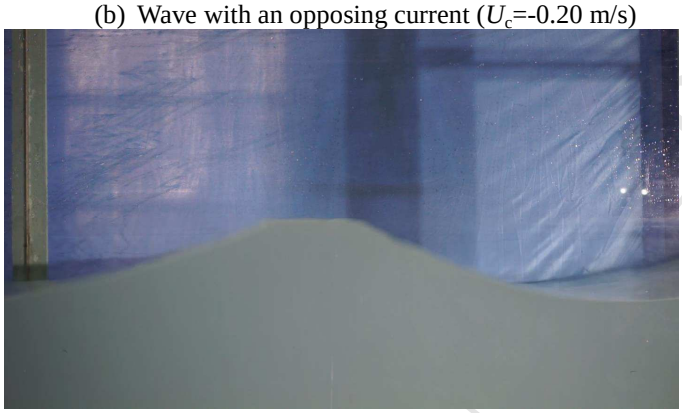

(c) Wave with an opposing current (U_c=-0.30 m/s)

Fig. 5. Typical snapshots of the wave profiles under the conditions of: (a) wave-only; (b) U_c=-0.20 m/s; and (c) U_c=-0.30 m/s. (Waves: h=0.5 m, T=1.2 s, H_0=10.2 cm)

3.2. Wave-induced pore-pressures

Figs. 6 (a) and 6(b) give the time series of the measured free surface elevation relative to the static water level and corresponding excess pore-pressure responses at the same measuring section under wave-only and waves with a following-current, respectively. As shown in the figures, both the wave profile and wave-induced instantaneous pore-pressure present a sinusoidal variation. No excess pore-pressure accumulation can be found in the present sandy seabed under the examined hydrodynamic loads. This absence of pore-pressure accumulation should be attributed to the relatively large permeability of the soil (k_s=1.84×10^{-4} m/s, c_v=0.66) and apparently smaller wave-induced shear stress in the soil compared with that in a typical prototype condition (Jeng and Seymour, 2007 or Figure 2.11 in Jeng (2018)).

The wave-induced pore-pressure at the surface of the sandy seabed (p_1) has the same phase with the free surface elevation. An evident phase lag can be observed among the pore-pressure responses measured at three different soil depths (p_1, p_2 and p_3, refer to Fig. 1 for the detailed locations). The analysis of Yamamoto et al. (1978) indicates that no phase lag would occur in a completely saturated infinite seabed, because the wave-induced pore pressures and effective stresses are independent of soil characteristics in such a condition. However, this conclusion was based on the case of infinite seabed. As reported in Jeng and Hsu (1996), the conclusion from Yamamoto et al. (1978) is no longer valid for a seabed finite thickness, because the soil characteristics directly affect the pore pressures and effective stresses and cause minor phase lag even for nearly saturated seabed. This physical process is attributed to the multi-phase flow in a porous medium. Furthermore, this phenomenon only occurs in fine sand such as the present tests (Jeng and Hsu, 1996). The comparison between Fig. 6(a) and 6(b) indicates that superimposing a following-current upon waves has a minor effect on the phase lag of the excess pore-pressure responses in the sandy seabed.

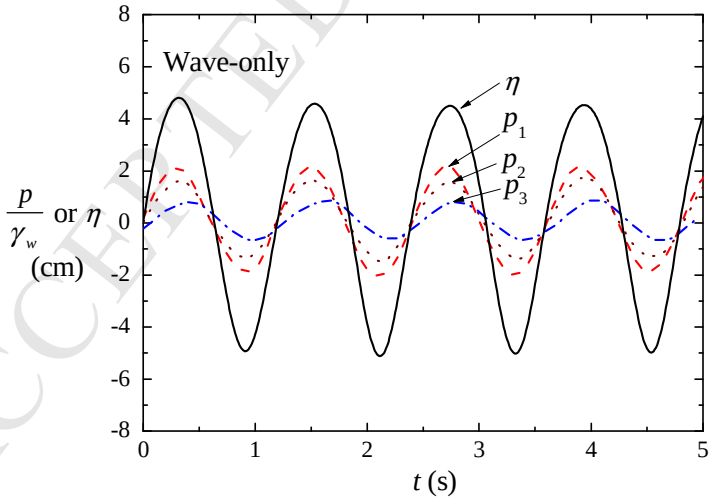

(a)

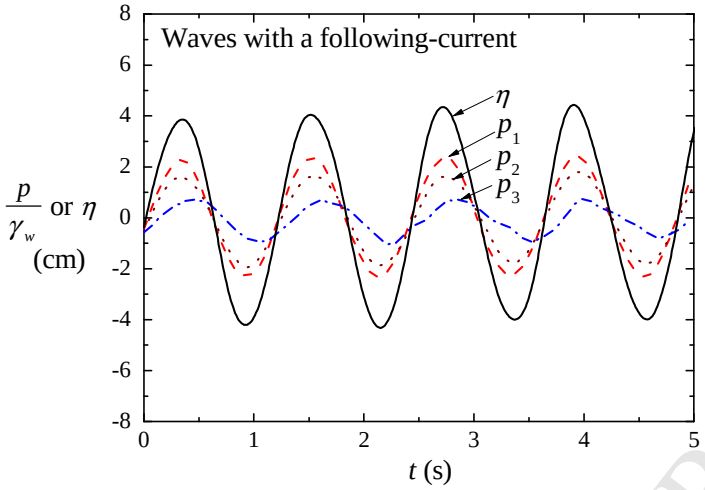

(b)

Fig. 6. Time series of free surface elevation relative to the static water level (η) measured with WHG-III and excess pore-pressure measured with PPT1 (p_1), PPT2 (p_2) and PPT3 (p_3): (a) wave-only; and (b) waves with a following-current. (Waves: h=0.5 m, T=1.2 s, H_0=9.5 cm; current: U_c=0.25 m/s)

Fig. 7 illustrates the distributions of the excess pore-pressure amplitude ($|p|/p_{0\text{-wm}}$, where $p_{0\text{-wm}}$ is the measured amplitude of the wave-induced pore-pressure at mudline under wave-only) along the soil depth (k_0z) under different combinations of waves and current loadings. It is shown that if a following-current is superimposed onto waves, the excess pore-pressure amplitudes in the sandy seabed generally increase. In contrast, an opposing-current would decrease the excess pore-pressure amplitudes in the sandy seabed. Specifically, the increment/reduction of the pore-pressure amplitude at mudline due to a following/opposing-current of $|U_c|$=0.30 m/s can be up to 35%/24%.

It is also observed from Figure 7 that the excess pore-pressure gradients in the seabed would generally be increased/reduced by a following/opposing-current. These results indicate that the liquefaction or partial liquefaction is more likely to occur under combined waves and following-current loading, while the opposing-current is beneficial to prevent the seabed to liquefying. That is, a following-current might be a potential risk for the safety of offshore structures. Moreover, the excess pore-pressure gradients would exert lifting force onto the sand grains under the wave-troughs and thereby might bring the sand more susceptible to scour. Although the value of the gradient variation caused by superimposing a current are not

large in the present experiments, it could become significant in a real ocean environment where the wave height and wave period can be more than 10 times greater than those in the flume experiment.

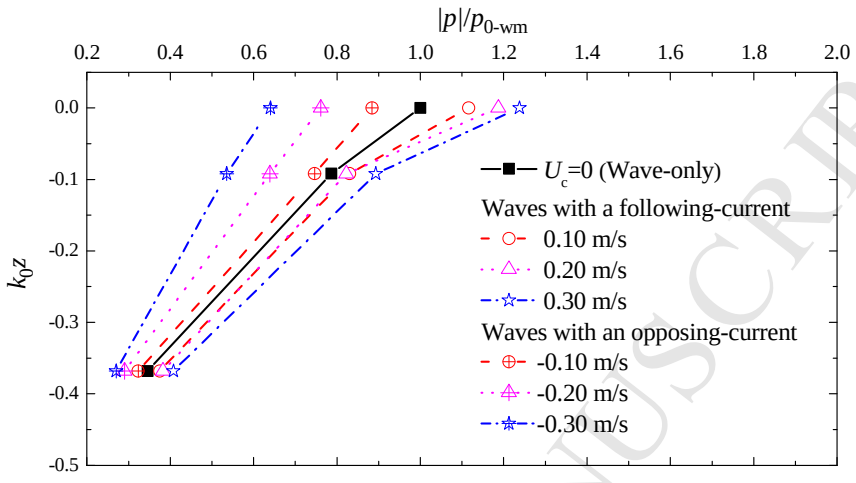

Fig. 7. Effects of a following/opposing-current with various velocities on the vertical distributions of the excess pore-pressure amplitude along the soil depth. (T=1.2 s, H_0=9.5 cm)

The effects of a following/opposing-current ($|U_c|$=0.25 m/s) on the distributions of the excess pore-pressure amplitude under various wave periods are compared in Fig. 8. Note that unlike Fig. 7, the normalized excess pore-pressure amplitude is expressed as $p/\gamma_w H_0$ and the normalized soil depth is expressed as z/H_0 in Fig. 8, since the values of $p_{0\text{-wm}}$ and k_0 vary with wave period. It is indicated that as wave period increases, the current-induced difference of the excess pore-pressure amplitude gradually becomes small. Under the conditions of T=1.0 s and 1.2 s, the magnitude of the following-current induced enlargement of the excess pore-pressure amplitude is obviously smaller than the opposing-current induced reduction of the excess pore-pressure amplitude. Under the conditions of T=1.4 s and 1.6 s, the effects of the following-current are small but observable, while the effects of the opposing-current seem to be negligible.

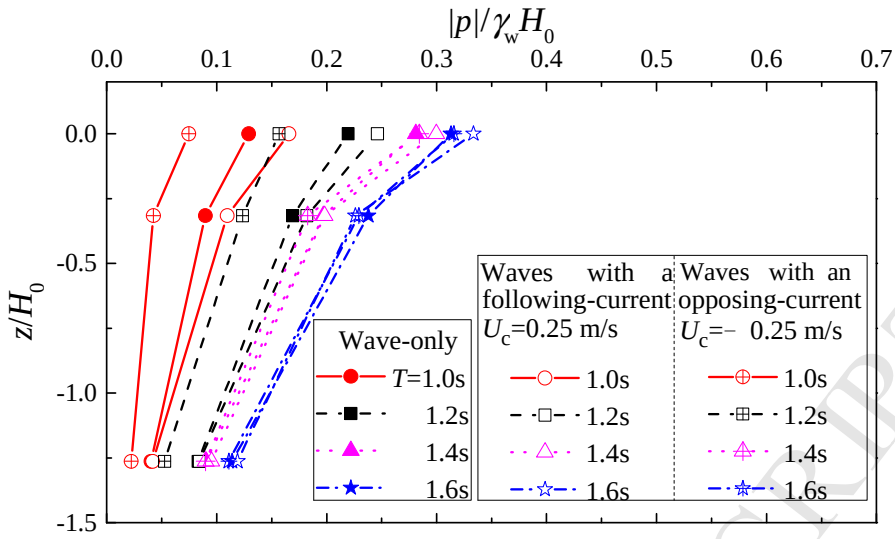

Fig. 8. Comparison of vertical distributions of the excess pore-pressure amplitude along soil depth between the conditions of wave-only, waves with a following-current (U_c=0.25 m/s), and waves with an opposing-current (U_c=-0.25 m/s) for various wave periods. (H_0=9.5 cm)

3.3. Comparisons between experimental and analytical results

As aforementioned, Zhang et al. (2013) proposed an analytical solution for the wave-induced pore-pressure responses in the seabed under combined waves and current. In their model, the third-order approximation of the wave–current interactions proposed by Hsu et al. (2009) was employed for the dynamic wave pressure acting on the seabed. As shown in Fig.2, the third-order Stokes wave theory is in accord with the practical wave conditions in the present flume tests. The dynamic wave pressure acting on the seabed is expressed as (Ye and Jeng, 2012)

$$P_b(x,t) = P_1\cos(k_0x-\omega t) + P_2\cos 2(k_0x-\omega t) + P_3\cos 3(k_0x-\omega t) \tag{3}$$

where $P_1=\dfrac{\rho_f g H_0}{2\cosh k_0h}\left\{1-\dfrac{\omega_2 {k_0}^2 {H_0}^2}{2(U_ck_0-\omega_0)}\right\}$, $P_2=\dfrac{3\rho_f {H_0}^2}{8}\left\{\dfrac{\omega_0(\omega_0-U_ck_0)}{2\sinh^4(k_0h)}-\dfrac{gk_0}{3\sinh 2k_0h}\right\}$,

$P_3=\dfrac{3\rho_f k{H_0}^3\omega_0(\omega_0-U_ck_0)}{512}\dfrac{9-4\sinh^2(k_0h)}{\sinh^7(k_0h)}$, and ρ_f is the water density. The dispersion relationship is given as

$$\omega = \omega_0 + (k_0 H_0)^2 \omega_2 \tag{4}$$

where $\omega_0 = U_c k_0 + \sqrt{g k_0 \tanh k_0 h}$ and $\omega_2 = \dfrac{9 + 8\sinh^2(k_0 h) + 8\sinh^4(k_0 h)}{64\sinh^4(k_0 h)}(\omega_0 - U_c k_0)$.

Taking Eq. (3) as a boundary condition at the mudline and based on the quasi-static Biot's consolidation equations (Biot, 1941), the excess pore-pressure for a uniform and isotropic seabed can be derived as (Zhang et al., 2013)

$$P = \sum_{m=1}^{3} \frac{P_m}{1-2\mu}\left[(1-2\mu-\alpha)C_{1m}e^{mk_0 z} + \frac{\delta_m^2 - m^2 {k_0}^2}{mk_0}(1-\mu)C_{2m}e^{\delta_m z}\right]e^{im(k_0 x - \omega t)} \tag{5}$$

where $\alpha = \dfrac{(1-2\mu)n\beta}{n\beta + (1-2\mu)/G}$, $\delta_m^2 = m^2 {k_0}^2 - \dfrac{im\omega\rho_f g}{k_s}\left\{n\beta + \dfrac{1-2\mu}{2G(1-\mu)}\right\}$,

$C_{1m} = \dfrac{\delta_m - \delta_m\mu + mk_0\mu}{\delta_m - \delta_m\mu + mk_0\mu + mk_0\alpha}$, $C_{2m} = \dfrac{mk_0\alpha}{(\delta_m - mk_0)(\delta_m - \delta_m\mu + mk_0\mu + mk_0\alpha)}$, μ is the Poisson ratio, n is the soil porosity, β is the compressibility of pore fluid, G is the shear modulus of the soil, and k_s is the soil permeability.

Fig. 9 gives the comparison of the vertical distributions of the excess pore-pressure amplitude ($|p|/p_{0\text{-wa}}$, where $p_{0\text{-wa}}$ is the analytically calculated amplitude of the wave-induced pressure fluctuation at the mudline under wave-only) along the soil depth ($k_0 z$) between experimental results and analytical solutions calculated with Eq. (5). The values of the input parameters for the analytical solutions are shown in Table 2. The degree of saturation is a key influencing factor for determining the distribution of the wave-induced pore-pressure (Okusa, 1985; Sakai et al., 1992). Nevertheless, the specific value of the degree of saturation is difficult to measure accurately (Michallet et al., 2009). In the present comparison study, the experimental data for the conditions of wave-only are utilized to calibrate the value of the degree of saturation (see Figs. 9 and 11(a)). It is proved that the value of S_r=0.995 would generally make the analytical results coincide well with the experimental results. Note that the amplitude of the wave-induced pressure fluctuation at the mudline is only influenced by wave parameters and irrelevant to the seabed properties. As such, the deviations of the wave-

induced pressure fluctuation at the mudline between analytical and experimental results are intrinsic and unaffected by the calibrated value of the degree of saturation.

Fig. 9 shows that the variation trend of the distributions of the excess pore-pressure amplitude calculated with the analytical solution is generally consistent with the experimental data. By comparing Fig. 9(a) with Fig. 9(b), it can be seen that certain deviations exist between the flume results for excess pore-pressure and the analytical solutions, which is nonnegligible especially for the opposing-current case. The relatively larger deviations for the opposing-current cases can be mainly attributed to the intrinsic difference between the measured amplitude of the wave-induced pressure fluctuation at the mudline and the analytical one (see Fig. 9(b)).

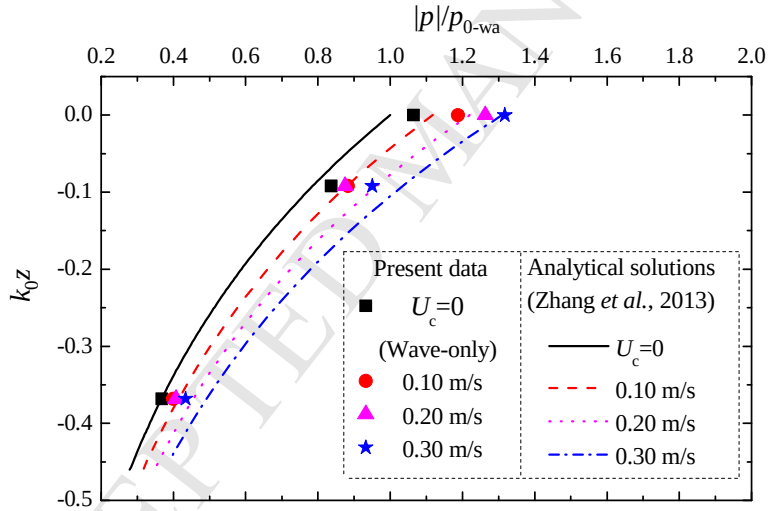

(a)

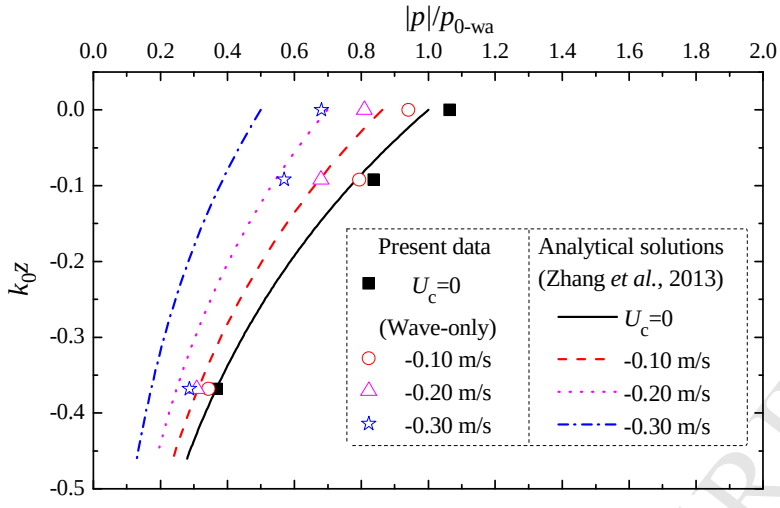

(b)

Fig. 9. Comparisons of the vertical distributions of the excess pore-pressure amplitude along the soil depth between experimental results and analytical solutions under (a) waves with a following-current (various current velocities); and (b) waves with an opposing-current (various current velocities). (h=0.5 m, T=1.2 s, H_0=9.5 cm).

Table 2. Values of the input parameters for the analytical solutions.

	Parameters	Values
Seabed properties	Coefficient of permeability k_s (m/s)	1.88×10^{-4}
	Shear modulus G (MPa)	10.0
	Void ratio e	0.771
	Poisson ratio of soil ν	0.30
	Degree of saturation S_r	0.995
Wave parameters	Water depth h (m)	0.5
	Wave height H_0 (cm)	9.5
	Wave period T (s)	1.2 (Various in Fig. 11)

To clarify the fact that the difference between the measured amplitude and the analytically calculated amplitude of the wave-induced pore-pressure at mudline under waves with an opposing-current is larger than that under waves with a following-current, supplementary measurements for the velocity profiles of the boundary layer under conditions

of wave-only, current-only, waves with a following-current, and waves with an opposing-current, were conducted. The flow velocity measured at z=0.25 m under current-only (U_c) is 0.20m/s. The wave period is 1.5 s and the wave height under wave-only (H_0) is 7.2cm. The sampling duration of each case was 5 min (approximately 200 wave cycles) with a sampling frequency of 100 Hz in order to have a statistically time independent average velocity (or phase-averaged velocity). The measured (phase-averaged) peak velocity profiles along the water depth under wave-only (U_{wp}), current-only (U_{cp}), waves with a following-current (U_{wp+cp}), and waves with an opposing-current (U_{wp-cp}), are shown in Fig. 10. The actual velocity profiles under waves and a following-current were found obviously different from those suggested by a linear superposition of wave-only and current-only velocities.

While analytically calculating the amplitude of the wave-induced pressure fluctuation at the mudline after Hsu et al. (2009) and Ye and Jeng (2012), the current was assumed to be uniform and the measured flow velocity at z=0.25m under current-only (U_c) was chosen as the input value of the current velocity. However, there exists a significantly thick boundary layer in the current (see Fig. 4) and thus the input velocity at z=0.25m for the analytical calculation would be much greater than the actual average current velocity. This could be the reason that the analytically calculated amplitude of the wave-induced pressure fluctuation at the mudline is much smaller than the measured one under waves with an opposing-current. For the cases of waves with a following-current, Fig. 10 indicates that the maximum flow velocities are much larger than those for opposing-current cases and also the sum of wave and current, which is consistent with the result of Kemp and Simons (1982; 1983), Olabarrieta et al. (2010) and Qi and Gao (2014). This enhancement of flow velocities near the seabed could somehow compensate the difference between the input current velocity for analytical calculation and the actual current velocity considering boundary layer. As a result, the deviation of the analytically calculated amplitude of the wave-induced pore-pressure at mudline from the measured one under waves with a following-current is much smaller compared with the cases of waves with an opposing-current.

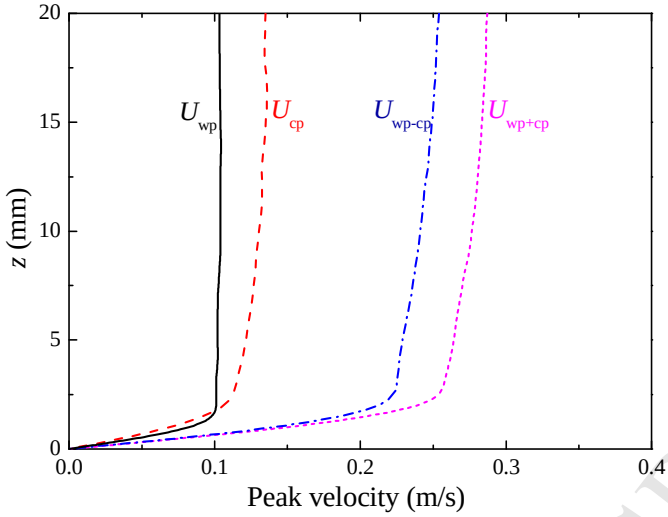

Fig. 10. Comparisons of the profiles for peak velocities between the conditions of wave-only, current-only, waves with an opposing-current and waves with a following current. (Waves: h=0.5 m, T=1.2 s, H_0=10.2 cm; current: U_c=0.20 m/s)

The third-order approximation proposed by Hsu et al. (2009) was based on the potential flow theory, which cannot describe the boundary layer flow along the seabed surface. To further confirm the aforementioned conjectured effects of the boundary layer on the combined wave-current induced pore-pressure responses in the seabed, several numerical simulations in which the boundary layer of the wave and/or current can be generated were carried out. In the numerical model, a hydrodynamic model based on the finite volume method and volume-averaged Reynolds-averaged Navier-Stokes equation (del Jesus et al., 2012) is developed to investigate the interactions between the third-order wave and shear current, while the quasi-static Biot equation (Biot, 1941) is adopted to describe the mechanical behaviour of a hydraulically isotropic porous elastic seabed in the open-source CFD toolbox Open-FOAM. The dynamic wave pressure extracted from the hydrodynamic model is utilized as the boundary condition at the seabed surface for the seabed model. In this model, the bottom boundary layer near the seabed surface is included in the numerical simulation. More detailed descriptions with respect to the numerical model can be found in Liang and Jeng (2018).

The comparison of the vertical distributions of the excess pore-pressure amplitude along the soil depth between experimental results, analytical solutions calculated with Eq. (5) and

aforementioned numerical simulations are provided in Fig. 11. The values of the input parameters for the analytical solutions and numerical simulations are shown in Table 2. The most important finding from Fig. 11 is that the magnitude of the pore-pressure amplitude at the seabed obtained by numerical simulations are generally much closer to the experimental data compared with the results of analytical solutions, especially under the conditions of waves with an opposing-current. This observation explicitly highlights the effects of boundary layer on the combined wave-current induced pore-pressure responses in the seabed. It is noted that observable deviation of the pore-pressure amplitude at the seabed still exists between the experimental results and the numerical simulations, mostly due to the difficulties of reproducing all the important characteristics of wave and/or current boundary layer and wave-current interactions in the present numerical hydrodynamic model.

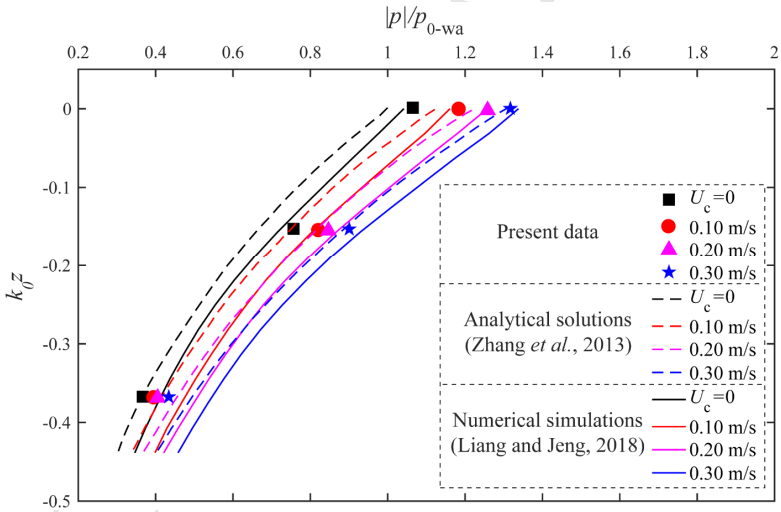

(a)

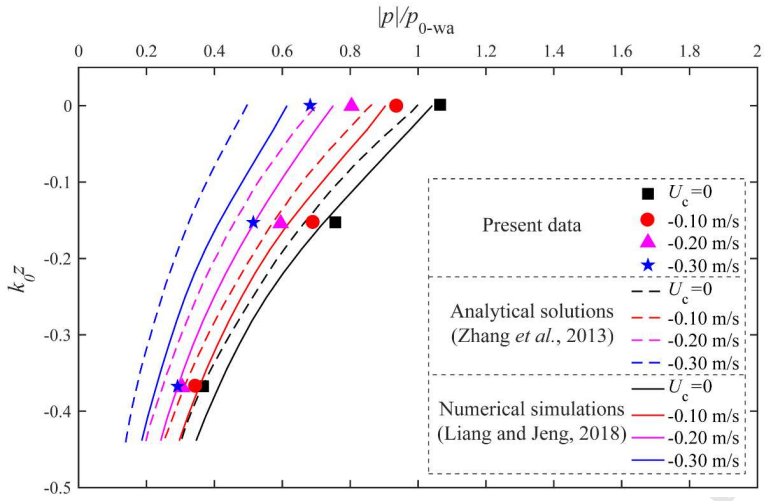

(b)

Fig. 11. Comparisons of the vertical distributions of the excess pore-pressure amplitude along the soil depth between experimental results, analytical solutions and numerical simulations under (a) waves with a following-current (various current velocities); and (b) waves with an opposing-current (various current velocities). (h=0.5 m, T=1.2 s, H_0=9.5 cm).

The comparisons between the measured vertical distributions of the excess pore-pressure amplitude and the analytical ones along the soil depth under various wave periods are given for the cases of wave-only, waves with a following-current and waves with an opposing-current in Figs. 12(a), 12(b) and 12(c), respectively. It is shown that in terms of the amplitude of the wave-induced pressure fluctuation at the mudline, the analytical and experimental results are generally consistent under wave-only (see Fig. 12(a)). Nevertheless, the analytical ones are a bit larger than the experimental ones under waves with a following current, whilst much smaller than the experimental ones under waves with an opposing-current. Focusing on the attenuation rate of the pore-pressure along the soil depth (or the general profile of the pore-pressure normalized with pore-pressure at the seabed surface), Figs. 12(a) and 12(b) indicate that the analytical and experimental results generally match well for the cases of wave only and waves with a following-currents.

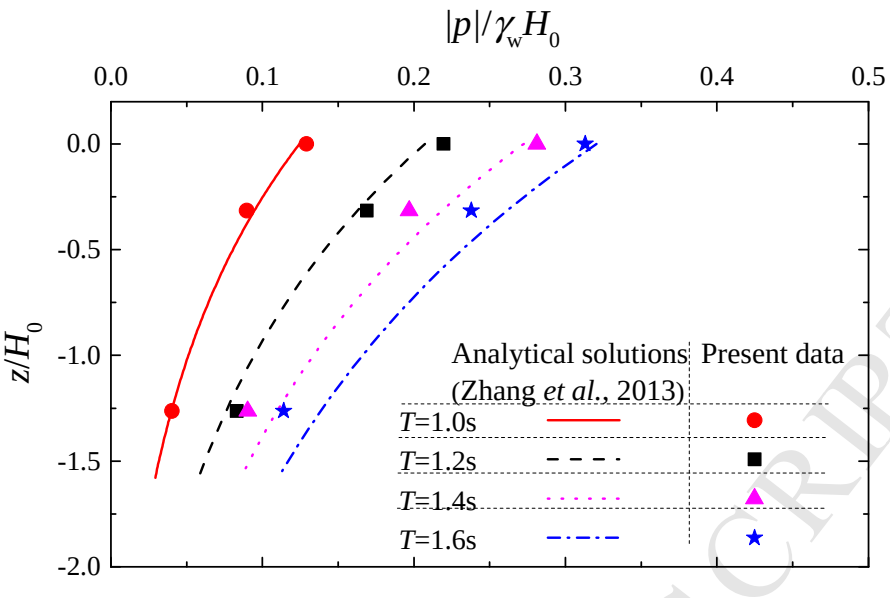

443

444 (a)

445

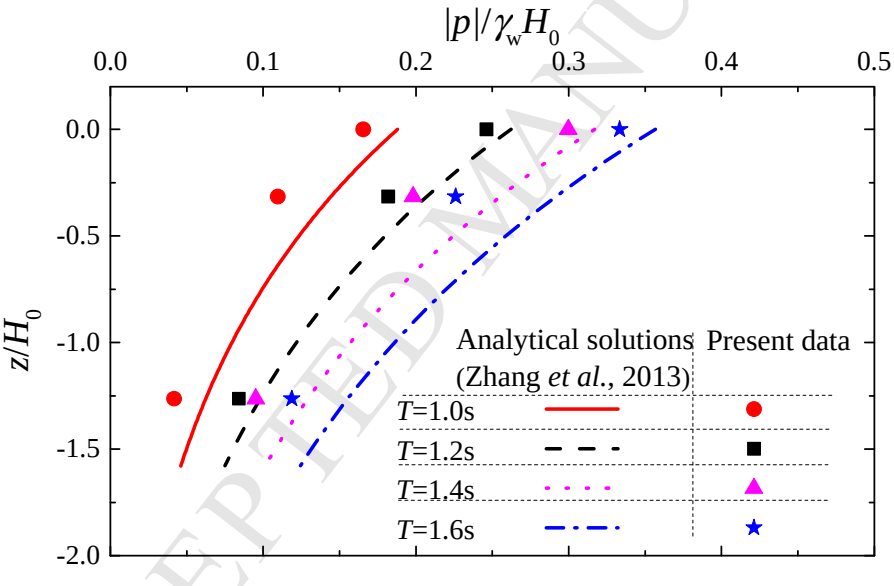

446

447 (b)

448

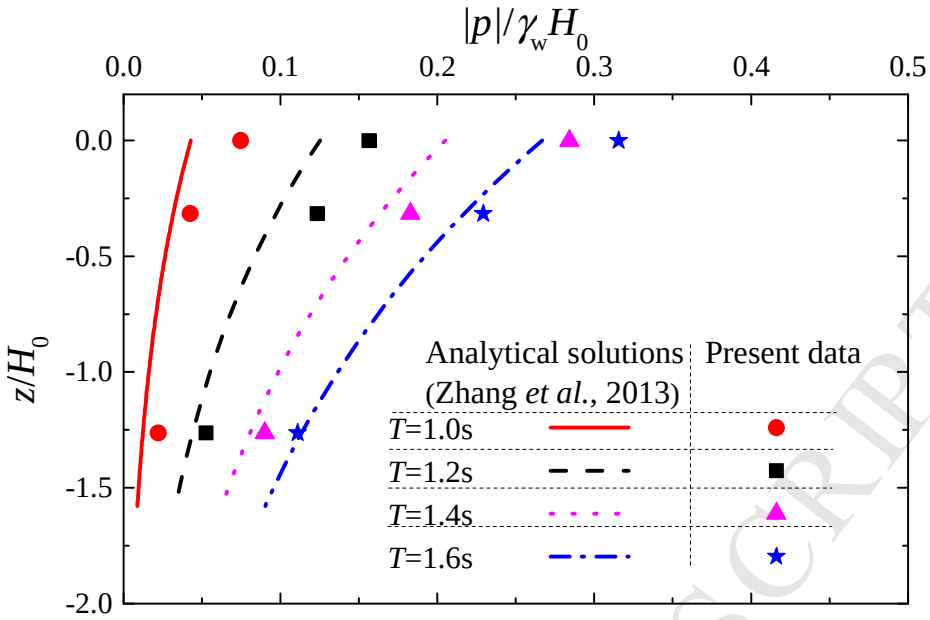

(c)

Fig. 12. Comparisons of the vertical distributions of the maximum pore-pressure along the soil depth between experimental results and analytical solutions under (a) wave-only; (b) waves with a following-current (U_c=0.25 m/s); and (c) waves with an opposing-current (U_c=-0.25 m/s). (Various wave periods, wave height H_0=9.5 cm)

The present flume observations indicated that superimposing a steady current on waves could significantly alter the pressure on the sand-bed surface. The deviation of the measured excess pore-pressure from analytical solutions can be mainly attributed to the difference between the measured pore pressure amplitude at the mudline (denoted as $p_{0-\mathrm{m}}$) and the analytical one ($p_{0-\mathrm{a}}$). Fig. 13 gives the variation of $p_{0-\mathrm{m}}/p_{0-\mathrm{a}}$ with the ratio of wave steepness under combined waves and current to that under wave-only (ξ/ξ_0). ξ/ξ_0 indicates the effect of a current on the wave steepness. A general and consistent trend, i.e., the value of $p_{0-\mathrm{m}}/p_{0-\mathrm{a}}$ is obviously larger than 1.0 and keep increasing with increasing value of ξ/ξ_0 when $\xi/\xi_0>1$ (i.e. opposing-current cases) while the value of $p_{0-\mathrm{m}}/p_{0-\mathrm{a}}$ is generally around 1.0 when $\xi/\xi_0\le 1$ (i.e. wave-only and following-current cases), is indicated in Fig. 13. This trend implies that in terms of the combined wave-current induced

468 excess pore-pressure in a sandy seabed, a favorable prediction by analytical solution should
469 be expected for following-current cases and smaller pore-pressure amplitudes would be
470 obtained for opposing-current cases, which has been confirmed by Figs. 9 and 12. While
471 evaluating the potentially enhanced risk for the safety of offshore structures by a following-
472 current, the analytical solution would provide a conservative/safe prediction.

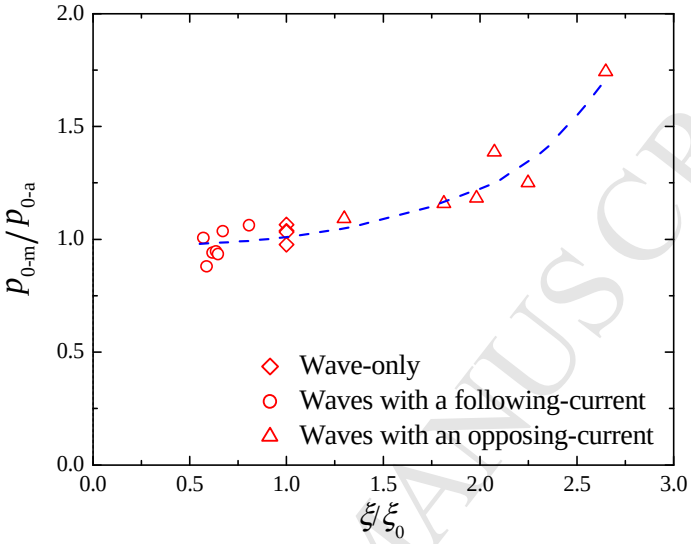

473

474 Fig. 13. The variation of $p_{0-\mathrm{m}}/p_{0\text{-a}}$ with ξ/ξ_0 ($H_0/gT^2 = 0.0038 \sim 0.0097$,

475 $h/gT^2 = 0.0199 \sim 0.0510$).

476 **4. Conclusions**

477 The co-existence of waves and current in offshore environments is a common scenario in
478 coastal zones. A series of flume tests were conducted to investigate the effect of imposing
479 following/opposing current upon waves on the excess pore-pressure in the sandy seabed. This
480 study provide the first set of comprehensive experimental data for the pore-water pressures in
481 a porous seabed due to combined waves and currents. Based on flume observations and
482 comparisons with the existing theoretical solution, the following conclusions are drawn:

483 (1) The essential difference of the pore-pressure responses between wave-only condition and
484 combined wave-current condition is due to the different boundary conditions of pressure
485 at the seabed surface. The excess pore-pressure amplitudes are increased for the
486 following-current case, but reduced for the opposing-current case. For the examined

value range, such wave-current combination effect becomes more significant for shorter wave periods. The excess pore-pressure gradients in the seabed would be enhanced/reduced by a following/opposing-current.

(2) The variation trend of the excess pore-pressure distribution in the present flume observations is consistent with that of the existing theoretical solutions. Nevertheless, certain deviations exist between the flume results for excess pore-pressure and the analytical solutions, which is nonnegligible especially for the opposing-current case. The apparently larger deviations under waves with an opposing-current can be mainly attributed to the intrinsic difference between the analytically calculated amplitude of the wave-induced pressure fluctuation at the mudline and the measured one.

(3) Measurements for the velocity profiles of the boundary layer shows that the maximum flow velocities under waves with a following-current are much larger than those for opposing-current cases and also the sum of wave and current. This enhancement of flow velocities near the seabed under waves with a following-current could compensate the overestimated input current velocity for analytical calculation induced by a boundary layer. Therefore, the deviation between the analytically calculated amplitude of the wave-induced pressure fluctuation at the mudline and the measured one under waves with a following-current is much smaller than the cases of waves with an opposing-current. The effects of boundary layer on the combined wave-current induced pore-pressures in the seabed are highlighted by supplementary numerical simulations.

(4) A general and consistent variation trend of $p_{0-\mathrm{m}}/p_{0-\mathrm{a}}$ with the ratio of wave steepness under combined waves and current to that under wave-only is indicated based on the present experimental results. A favorable prediction by the analytical solution would be expected for following-current cases and smaller pore-pressure amplitudes would be obtained for opposing-current cases. Therefore, while evaluating the potentially enhanced risk for the safety of offshore structures by a following-current, the analytical solution would provide a conservative/safe prediction.

Acknowledgements

This work was financially supported by the National Natural Science Foundation of China (Grant Nos. 11602273; 11825205), the Strategic Priority Research Program (Type-B) of CAS (Grant No. XDB22030000) and the Youth Innovation Promotion Association CAS. Techinical support from Mr. Fulin Zhang for the large flume tests is greatly appreciated. The authors would also like to thank the anonymous reviewer for constructive comments and suggestions for improvement of the final manuscript.

References

[1] Bea, R.G., Wright, S.G., Sircar, O.P., Niedoroda, A.W., 1975. Wave-induced slides in south pass block 70, Mississippi Delta. Journal of Geotechnical Engineering, ASCE 109(1), 617–644.

[2] Biot, M.A., 1941. General theory of three-dimensional consolidation. Journal of Applied Physics 26(2), 155-164.

[3] Biot, M.A., 1960. Mechanics of deformation and acoustic propagation in porous media. Journal of Applied Physics 33, 1483-1498.

[4] Chang, S.C., Lin, J.G., Chien, L.K., Chiu, Y.F., 2007. An experimental study on non-linear progressive wave-induced dynamic stresses in seabed. Ocean Engineering 34(17), 2311-2329.

[5] Chowdhury, B., Dasari, G.R., Nogami, T., 2006. Laboratory study of liquefaction due to wave-seabed interaction. Journal of Geotechnical and Geoenvironmental Engineering, ASCE 132 (7), 842–851.

[6] Cuéllar, P., Baeßler, M., Rücker, W., 2012. Pore-pressure accumulation and soil softening around pile foundations for offshore wind turbines. ASME 2012 International Conference on Ocean, Offshore and Arctic Engineering, 219–228.

[7] De Groot, M.B., Kudella, M., Meijers, P., Oumeraci, H., 2006. Liquefaction phenomena underneath marine gravity structures subjected to wave loads. Journal of Waterway Port

Coastal & Ocean Engineering 132(4), 325-335.

[8] de Groot, M.B., Meijers, P., 1992. Liquefaction of trench fill around a pipeline in the seabed. Proc., Conf. on the Behavior of Offshore Structures, London, 1333–1344.

[9] del Jesus, M., Lara, J.L. and Losada, I.J., 2012. Three-dimensional interaction of waves and porous coastal structures: Part I: Numerical model formulation. Coastal Engineering 64, 57-72.

[10] Hsu, H.C., Chen, Y.Y., Hsu, J.R.C., Tseng, W.J., 2009. Nonlinear water waves on uniform current in Lagrangian coordinates. Journal of Nonlinear Mathematical Physics 16, 47-61.

[11] Hsu, J.R.C., Jeng, D.-S., 1994. Wave-induced soil response in an unsaturated anisotropic seabed of finite thickness. International Journal for Numerical and Analytical Methods in Geomechanics 18(11), 785-807.

[12] Jeng, D.-S., 2003. Wave-induced sea floor dynamics. Applied Mechanics Reviews 56(4), 407-429.

[13] Jeng, D.-S., 2013. Porous Models for Wave-seabed Interactions. Springer, Heidelberg.

[14] Jeng, D.-S., 2018. Mechanics of wave-seabed-structure interactions: Modelling, processes and applications. Cambridge University Press, Cambridge.

[15] Jeng, D.-S., Hsu, J.R.C., 1996. Wave-induced soil response in a nearly saturated seabed of finite thickness. Géotechnique 46(3), 427-440.

[16] Jeng, D.-S. , Seymour, B.R., 2007. Simplified analytical approximation for pore-water pressure buildup in marine sediments. Journal of Waterway Port Coastal and Ocean Engineering 133(4), 309-312.

[17] Kemp, P.H., Simons, R.R., 1982. The interaction between waves and a turbulent current: Waves propagating with the current. Journal of Fluid Mechanics 116, 227-250.

[18] Kemp, P.H., Simons, R.R., 1983. The interaction between waves and a turbulent current: Waves propagating against the current. Journal of Fluid Mechanics 130, 73-89.

[19] Le Méhauté, B., 1976. An Introduction to Hydrodynamics and Water Waves. Springer, Heidelberg.

[20] Liang, Z.D., Jeng, D.-S., 2018. A three-dimensional model for the seabed response induced by waves in conjunction with currents in the vicinity of an offshore pipeline using

OpenFOAM. International Journal of Ocean and Coastal Engineering. (Accepted)

[21] Liao, C.C., Jeng, D.-S., Zhang, L.L., 2013. An analytical approximation for dynamic soil response of a porous seabed due to combined wave and currents loading. Journal of Coastal Research 315(5), 1120-1128.

[22] Liao, C.C., Tong, D., Jeng, D.-S., Zhao, H., 2018a. Numerical study for wave-induced oscillatory pore pressures and liquefaction around impermeable slope breakwater heads. Ocean Engineering, 157, 364-375.

[23] Liao, C., Tong, D., Chen, L., 2018b. Pore pressure distribution and momentary liquefaction in vicinity of impermeable slope-type breakwater head. Applied Ocean Research, 78, 290-306.

[24] Lin, Z.B., Pokrajac, D., Guo, Y.K., Jeng, D.-S., Tang, T., & Rey, N., et al., 2017. Investigation of nonlinear wave-induced seabed response around mono-pile foundation. Coastal Engineering, 121, 197-211.

[25] Liu, B., Jeng, D.-S., Ye, G.L., Yang, B., 2015. Laboratory study for pore pressures in sandy deposit under wave loading. Ocean Engineering. 106, 207–219.

[26] Madsen, O.S., 1978. Wave-induced pore-pressures and effective stresses in a porous bed. Géotechnique 28(4), 377-393.

[27] Michallet, H., Mory, M., Piedra-Cueva, I., 2009. Wave-induced pore-pressure measurements near a coastal structure. Journal of Geophysical Research 114(C6), C06019.

[28] Moreira, R.M., Peregrine, D.H., 2012. Nonlinear interactions between deep-water waves and currents. Journal of Fluid Mechanics 691(1), 1-25.

[29] Okusa, S. 1985. Wave-induced stress in unsaturated submarine sediments. Géotechnique, 35(4), 517-532.

[30] Olabarrieta, M., Medina, R., Castanedo, S., 2010. Effects of wave-current interaction on the current profile. Coastal Engineering 57, 643-655.

[31] Oumeraci, H., 1994. Review and analysis of vertical breakwater failures—lessons learned. Coastal Engineering 22(1-2), 3-29.

[32] Qi, W.G., Gao, F.P., Han, X.T., Gong, Q.X. 2012. Local scour and pore-water pressure around a monopile foundation under combined waves and current. Proceedings of the

Twenty-Second International Offshore and Polar Engineering Conference, 159–165.

[33] Qi, W.G., Gao, F.P., 2014. Physical modeling of local scour development around a large-diameter monopile in combined waves and current. Coastal Engineering 83, 72-81.

[34] Sakai, T., Hatanaka, K., Mase, H., 1992. Wave-induced effective stress in seabed and its instantaneous liquefaction. Journal of Waterway, Port, Coastal and Ocean Engineering, ASCE 118 (2), 202-206.

[35] Singh, S.K., Debnath, K., 2016. Combined effects of wave and current in free surface turbulent flow. Ocean Engineering 127, 170-189.

[36] Sumer, B.M., 2014. Liquefaction Around Marine Structures. World Scientific, Singapore.

[37] Tambroni, N., Blondeaux, P., Vittori, G., 2015. A simple model of wave-current interaction. Journal of Fluid Mechanics 775, 328-348.

[38] Tsui, Y.T., Helfrich, S.C.,1983. Wave-induced pore pressures in submerged sand layer. Journal of Geotechnical Engineering, ASCE 109(4), 603-618.

[39] Wen, F., Wang, J.H., Zhou, X.L., 2016. Response of saturated porous seabed under combined short-crested waves and current loading. Journal of Coastal Research 32(2), 286-300.

[40] Yamamoto, T., Koning, H.L., Sellmeijer, H., Hijum, E.V., 1978. On the response of a poro-elastic bed to water waves. Journal of Fluid Mechanics 87(01), 193-206.

[41] Ye, J.H., Jeng, D.-S., 2012. Response of porous seabed to nature loadings: waves and currents. Journal of Engineering Mechanics, ASCE 138(6), 601-613.

[42] Zhang, F., Ge, Z., 1996. A study on some causes of rubble mound breakwater failure. China Ocean Engineering 10(4), 473-481.

[43] Zhang, J.S., Li, Q.Z., Ding, C., Zheng, J.H., Zhang, T.T., 2016. Experimental investigation of wave-driven pore-water pressure and wave attenuation in a sandy seabed. Advances in Mechanical Engineering 8(6), 1-10.

[44] Zhang, J.S., Zhang, Y., Jeng, D.-S., Liu, L.F., Zhang, C., 2014. Numerical simulation of wave–current interaction using a RANS solver. Ocean Engineering 75, 157-164.

[45] Zhang, Q., Zhou, X.L., Wang, J.H., Guo, J.J., 2017. Wave-induced seabed response around an offshore pile foundation platform. Ocean Engineering 130, 567-582.

[46] Zhang, Y., Jeng, D.-S., Gao, F.P., Zhang, J.S., 2013. An analytical solution for response of a porous seabed to combined wave and currents loading. Ocean Engineering 57(57), 240-247.

[47] Zhai, Y., Zhang, J., Jiang, L., Xie, Q., Chen, H., 2018. Experimental study of wave motion and pore pressure around a submerged impermeable breakwater in a sandy seabed. International Journal of Offshore and Polar Engineering 28(1), 87-95.

[48] Zhou, X.L., Zhang, J., Guo, J.J., Wang, J.H., Jeng, D.-S., 2015. Cnoidal wave induced seabed response around a buried pipeline. Ocean Engineering 101, 118-130.

[49] Zou, Z.L., 2004. Water Wave Theories and Their Applications. Science China Press, Beijing (in Chinese).

Highlights:

- ✧ Flume observations of combined wave-current induced excess pore-pressure in a sand-seabed;
- ✧ Comparisons of wave-current induced pore-pressure between flume results and analytical solutions;
- ✧ Effects of non-lineartiy of wave-current interactions on the excess pore-pressure responses;
- ✧ Deviation between the flume results for excess pore-pressure and the analytical solutions has been identified.